

# Phase transitions and optimal algorithms in the semi-supervised classifications in graphs: from belief propagation to convolution neural networks

Pengfei Zhou

CAS Key Laboratory for Theoretical Physics, Institute of Theoretical Physics,  
Chinese Academy of Science, Beijing 100190, China and  
School of Physical Sciences, University of Chinese Academy of Sciences, Beijing 100049, China

Pan Zhang\*

CAS Key Laboratory for Theoretical Physics, Institute of Theoretical Physics,  
Chinese Academy of Science, Beijing 100190, China

(Dated: May 28, 2022)

By analyzing Bayesian inference of generative model for random networks with both relations (edges) and node features (discrete labels), we perform an asymptotically exact analysis of the semi-supervised classification problems on graph-structured data using the cavity method of statistical physics. We unveil detectability phase transitions which put fundamental limit on ability of classifications for all possible algorithms. Our theory naturally converts to a message passing algorithm which works all the way down to the phase transition in the underlying generative model, and can be translated to a *graph convolution neural network* algorithm which greatly outperforms existing algorithms including popular graph neural networks in synthetic networks. When applied to real-world datasets, our algorithm achieves comparable performance with the state-of-the-art algorithms. Our approach provides benchmark datasets with continuously tunable parameters and optimal results, which can be used to evaluate performance of exiting graph neural networks, and to find and understand their strengths and limitations. In particular, we observe that popular GCNs have sparsity issue and overfitting issue on large synthetic benchmarks, we also show how to overcome the issues by combining strengths of our approach.

## I. INTRODUCTION

Learning in graphs is an important task in machine learning and data science, with applications ranging from social science such as social network analysis, biology such as protein structure prediction and molecular finger prints learning, and computer science such as knowledge graph analysis. The key difference between learning in graph data and the conventional machine learning with images and natural languages is that in addition to complex features on each element, there are also relational features encoded by edges in the graph.

Consider a simple and classic example of classification of nodes into several groups in a citation network. In addition to the edges between nodes representing citations between documents, each node has features such as key words in the document, which reveals information of group labels. We consider the problem that for a small subset of nodes their group memberships are available, working as training data, and the task is to predict the group membership of other nodes using the training data, together their features and edges in graphs. This problem is known as *semi-supervised classification in graphs* which has drawn many attention in both networks science and machine learning communities. On this problem we witnessed the burst in developing *Graph Convolution neural Networks* (GCN) which gave groundbreaking performance in recent years [1].

The deep convolution neural networks [2] have made great success in machine learning and artificial intelligence. Since there are many applications that data are represented as a graph, rather than on the 2-dimensional grids, a lot of efforts has been made to extending the convolution networks from grid data to graph data, focusing on constructing linear convolution kernels to extract local features in graphs and on learning effective representations of the graph objects. During the past several years, many different GCNs have been proposed, using different kinds of convolution kernels, as well as different neural network architectures [1, 3–5]. In recent years, GCNs have quickly dominated the performances of various tasks such as object classification, link prediction, and graph level classification on graph data, and are also regarded to have a big potential on relational reasoning [6]. For the object classification, without depending on specific model, GCNs learn effective object representations with non-linear neural architectures, with the whole framework trained in an end-to-end fashion. Despite that GCNs have achieved state-of-the-art performance on semi-supervised classification, so far there are very little theoretical understanding on the mathematical principles behind the graph convolutions, and to what extent they can work on particular problem instance. The main difficulty is that GCNs are usually tested only on several classic real-world benchmark datasets, however perfectly modeling the real-world data sets is hard. So we are lack of controllable datasets with continuously tunable parameters for studying the strengths and limitations of GCNs.

\* panzhang@itp.ac.cn

In this article we propose to model the semi-supervised classification problem by combining the celebrated stochastic block models [7] (in the semi-supervised fashion) which generates relational edges, and bipartite stochastic block model [8, 9] which generates features of each node. We call the model Joint Stochastic Block Model (JSBM). The generated graph is a mixture of a uni-partite graph and a bi-partite graph, both of which carry information of group labels. To best of our knowledge, the JSBM was proposed in [8] for studying missing link and missing node predictions using both edges and labels based on MCMC based methods. In this article we focus on the semi-supervised learning in the JSBM, its theoretical properties and optimal algorithms.

On the graphs generated by the JSBM, the clustering and classification problems can be translated to a Bayesian inference problem which we aim to solving using statistical physics approaches in an asymptotically exact way. This leads to a message-passing algorithm, known in computer science as belief propagation (BP)[10] algorithm, that is asymptotically exact in large sparse random networks generated by the JSBM. Without semi-supervision, by analyzing stability of fixed points of the belief propagation algorithm, a phases transition — *detectability transition* is discovered beyond which no algorithm is able to do classification without supervision. It generalizes the celebrated detectability phase transition [11] in the stochastic block model [7] and puts fundamental limits on accuracy of the classifications in networks with both pairwise relations edges and node features in the JSBM. In the semi-supervised classification setting where a small fraction of node labels are known as training data, using method of pinning the labeled nodes as introduced in [12], our approach still gives Bayes optimal results. The parameters can be learnt using truncated belief propagation together with the back propagation algorithm. This naturally extends the belief propagation algorithm to a graph convolution network, which greatly outperforms existing graph convolution on synthetic graphs.

In addition to the theoretical analysis and algorithmic applications, the JSBM can produce well-controlled benchmark graphs with continuously tunable parameters, for benchmarking graph convolution networks, and for understanding their strengths and weaknesses under certain properties of graphs. For example, we discover that the existing state-of-the-art graph convolution networks have a sparsity issue and overfitting issue when applied on synthetic benchmarks. Based on the observation, we give explanations of the weakness of the GCNs based on spectral properties of the graph convolution kernels used by GCNs, and further suggestions on how to overcome the issues.

The paper is organized as follows. In Sec. II we introduce the joint stochastic block model. In Sec. III we translate the classification and clustering problems in the joint stochastic block model to the Bayesian inference problem, and derive an asymptotically optimal algorithm

belief propagation. In Sec. IV we study the detectability phase transitions of the JSBM using stability analysis of the belief propagation algorithm. In Sec. V we convert the belief propagation algorithm to a graph convolution neural network. In Sec. VI we evaluate the performance of our BPGCN and compare the performance with state-of-the-art graph convolution neural networks on both synthetic and real-world data sets.

## II. JOINT STOCHASTIC BLOCK MODEL

The purpose of the JSBM is to generate synthetic random graphs with  $n$  nodes with both edges and node features. Each node  $i$  has a pre-determined *hidden* label (i.e. ground-true group membership)  $t_i^* \in \{1, \dots, \kappa\}$  each of which is chosen randomly and independently with probability  $\alpha_t$  for group  $t$ . Then for each pair of nodes  $i, j$ , an edge  $(i, j)$  is connected with probability  $p_{t_i^*, t_j^*}$  and not connected with probability  $1 - p_{t_i^*, t_j^*}$ . In the sense of the statistical inference, the generating process is a measuring process of the signal (ground-true labels), finally producing edges as measuring results which encode information of ground-true labels. The properties of the connections, or adjacency matrix  $\mathbf{A}$  of the generated graph, is controlled by the  $\kappa \times \kappa$  matrix  $\mathbf{P}$ . If diagonal elements of  $\kappa$  is much larger than the off diagonal elements, there would be more edges connecting nodes in the same group than edges connecting different groups. The above process of generating edges so far is the same as the stochastic block model. An intuitive picture of the understanding generated network is a citation network, where nodes in the network represents research papers, each of which belongs to a certain research area denoted by labels, such as “physics”, or “history”. Apparently, articles belonging to the same category would citing more frequently than articles belonging to different categories.

In addition to edges, we consider further totally  $m$  distinct features, as another type of nodes, that we call *feature nodes*. As an example, in the citation networks, in addition to citations revealing research field information, each article also has a set of keywords, which also reveals labels of the node. Each feature node  $a$  also has a ground-true label  $t_a \in \{1, 2, \dots, \kappa\}$  analogous to graph node  $i$ , which is chosen randomly from  $\kappa$  labels with probability  $\beta_{t_a}$ . We then generate connections between a feature node  $a$  and a graph node  $i$  with probability  $q_{t_i^*, t_a}$ , and disconnect them with probability  $1 - q_{t_i^*, t_a}$ . Apparently, the connections in between graph nodes and feature nodes form a bipartite graph, with analogous generation process of the bipartite stochastic block model [9]. After all, the JSBM generates a graph that combines a uni-partite graph and a bipartite graph, similar to the graph appears in the semi-restricted Boltzmann machines [13]. In this picture, a feature  $a$  plays a role of hidden variable, or a functional node with a multi-variable interaction among the graph nodes connected to  $a$ , so we will also refer to the edges connecting a feature node to neighboring graph

node as *hyper edges*. Algebraically, the graph generated by JSBM can be represented by two matrix, a node-node adjacency matrix  $\mathbf{A} \in \{0, 1\}^{n \times n}$  with  $A_{ij} = 1$  denoting there is an edge between graph node  $i$  and graph node  $j$ , and a feature-node adjacency matrix  $\mathbf{F} \in \{0, 1\}^{n \times m}$ , with  $F_{ia} = 1$  denoting graph node  $i$  is connected to feature node  $a$  and 0 denoting no such connection. We notice that the JSBM was proposed in [8] for studying missing link and missing node predictions using both edges and labels (annotations) of each node.

### III. BAYESIAN INFERENCE OF THE JOINT STOCHASTIC BLOCK MODEL

The clustering problem defined in a graph  $\mathcal{G}$  generated by the JSBM is to recover as accurate as possible the ground-true labels  $\{t_i^*\}$  using edges and features; while the semi-supervised classification problem asks to do the recovery using edge, feature, together with a small amount of training labels  $\{t_i^*\}$  for  $i$  belonging to training set  $\Omega$ . If we know the parameters in generating the graph  $\theta = \{\mathbf{P}, \mathbf{Q}, \alpha, \beta\}$ , the tasks can be translated into an inference problem of reconstructing another set of hidden parameters of the model, the group labels  $\{t_i^*\}$  given measurement results on  $\{t_i^*\}$ . There are basically two kinds of inferences we can do for this task, the Max A Posterior (M.A.P.) (with Maximum Likelihood inference as a special case of using flat priors), and the Bayesian inference which amounts to computing the posterior distribution. In this work we consider the Bayesian inference which is Bayes optimal. Using Bayes rule, the posterior is written as

$$P(\{t_i\}|\mathcal{G}, \theta) = \frac{P(\mathcal{G}|\{t_i\}, \theta)P_0(\{t_i\})}{\sum_{\{t_i\}} P(\mathcal{G}|\{t_i\}, \theta)P_0(\{t_i\})}. \quad (1)$$

where  $P_0(\{t_i\})$  represents prior information we have on the node labels,  $P(\mathcal{G}|\{t_i\})$  is the likelihood of group labels  $\{t_i\}$ , which is product of probabilities of generating all edges and hyper edges.

$$P(\mathcal{G}|\{t_i\}) = \prod_i \alpha_{t_i} \prod_{(ij) \in \mathcal{E}} p_{t_i, t_j} \prod_{(ij) \notin \mathcal{E}} (1 - p_{t_i, t_j}) \cdot \prod_a \beta_{t_a} \prod_{(ia) \in \mathcal{F}} q_{t_i, t_a} \prod_{(ia) \notin \mathcal{F}} (1 - q_{t_i, t_a}), \quad (2)$$

where  $\mathcal{E}$  denotes the set of edges between graph nodes, and  $\mathcal{F}$  denotes the set of edges between graph nodes and feature nodes. The clustering problem corresponds to putting a flat prior, i.e.  $P_0(\{t_i\}) = \text{Constant.}$ , and the semi-supervised classification problem corresponds to putting a strong prior on the nodes in the training set to pin the marginals of the nodes in the direction of training labels, as proposed in [12].

It is well known that computing the normalization of the posterior distribution is a #P problem, so it is hopeless to find polynomial algorithms for solving it. Thus we

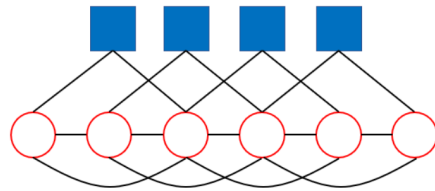


FIG. 1. Factor graph representation of the joint stochastic block model. The red circles represent graph nodes, and blue boxes represent feature nodes.

need efficient and accuracy approximations for the inference. In the language of statistical physics, the Bayesian inference problem of determining the posterior distribution (1) is a Boltzmann distribution at unit temperature: the negative log-likelihood  $-\log P(\mathcal{G}|\{t_i\})$  represent the energy; the evidence, i.e. the normalization constant  $\sum_{\{t_i\}} P(\mathcal{G}|\{t_i\}, \theta)$  for the posterior is the partition function; and the possible prior information plays a role of external fields acting on each graph node. For the clustering problem where we do not have any training labels, the external fields are set to zero; For the semi-supervised classification problems, the fields on the nodes belonging to the training set are set to infinity for pinning the nodes to the training labels [12].

For random sparse graphs the inference can be studied theoretically at the thermodynamic limit using the cavity method from statistical physics [10, 14]. If we known in prior the parameters  $\theta$  which has been used in generating the graph, the system is on the *Nishimori line* [15, 16] and no spin glass phase could appear. On a single instance, the replica symmetry cavity method naturally translates into the *belief propagation* (BP) algorithm, which passes messages along directed edges of the factor graph. The factor graph is illustrated in Fig. 1, where each edge represent a two-body factor, and each feature represents a multi-body factor. When the messages converge, they can be used to compute posterior marginals and the Bethe free energy.

From the algorithm point of view, the belief propagation adopts the Bethe approximation [10, 17]

$$P(\{t\}) = \frac{\prod_{ij} P_{ij}(t_i, t_j)}{\prod_i P_i^{d_i-1}(t_i)}, \quad (3)$$

as a variational distribution, and adjusts variational parameters, two-point marginals  $P_{ij}(t_i, t_j)$  and single point marginals  $P_i(t_i)$ , for minimizing the Bethe free energy. The final form of the belief propagation is written as iterative equations for three kinds of messages, which are listed as follows. We refer to detailed derivations as well as approximation applied to non-edges in the Appendices.

$$\begin{aligned}
\psi_{t_i}^{i \rightarrow j} &= \alpha_{t_i} \frac{e^{-h_{t_i}}}{Z^{i \rightarrow j}} \prod_{k \in \partial i \setminus j} \sum_{t_k} p_{t_i t_k} \psi_{t_k}^{k \rightarrow i} \prod_{a \in \partial i} \sum_{t_a} q_{t_i t_a} \psi_{t_a}^{a \rightarrow i} \\
\psi_{t_i}^{i \rightarrow a} &= \alpha_{t_i} \frac{e^{-h_{t_i}}}{Z^{i \rightarrow a}} \prod_{k \in \partial i} \sum_{t_k} p_{t_i t_k} \psi_{t_k}^{k \rightarrow i} \prod_{b \in \partial i \setminus a} \sum_{t_b} q_{t_i t_b} \psi_{t_b}^{b \rightarrow i} \\
\psi_{t_a}^{a \rightarrow i} &= \beta_{t_a} \frac{e^{-h_{t_a}}}{Z^{a \rightarrow i}} \prod_{j \in \partial a \setminus i} \sum_{t_j} q_{t_a t_j} \psi_{t_j}^{j \rightarrow a}.
\end{aligned} \tag{4}$$

Here,  $\psi_{t_i}^{i \rightarrow j}$  is the cavity marginals passing through graph node  $i$  to graph node  $j$ , representing probability of node  $i$  taking label  $t_i$  when node  $j$  is removed from the graph.  $\psi_{t_i}^{i \rightarrow a}$  is similar, but represents probability of node  $i$  taking label  $t_i$  when a feature  $a$  is removed from the graph; analogously,  $\psi_{t_a}^{a \rightarrow i}$  represents the probability of a feature  $a$  taking label  $t_a$  when graph node  $i$  is removed from the graph.  $Z^{i \rightarrow a}$ ,  $Z^{a \rightarrow i}$ , and  $Z^{i \rightarrow j}$  are normalizing factors ensuring a normalized probability;  $\partial i$  denotes the set of neighbors of node  $i$  in the graph. In the equations, variables  $h_{t_i}$  and  $h_{t_a}$  are adaptive fields contributed by the non-edges of the graph, they are derived in the Appendices, and can be formulated as

$$\begin{aligned}
h_{t_i} &= \sum_k \sum_{t_k} p_{t_i t_k} \psi_{t_k}^k + \sum_a \sum_{t_a} q_{t_i t_a} \psi_{t_a}^a \\
h_{t_a} &= \sum_j \sum_{t_j} q_{t_a t_j} \psi_{t_j}^j
\end{aligned} \tag{5}$$

Once above iterative equations converge (i.e. messages do not change significantly), we can estimate posterior marginals using

$$\begin{aligned}
\psi_{t_i}^i &= \alpha_{t_i} \frac{e^{-h_{t_i}}}{Z^i} \prod_{k \in \partial i} \sum_{t_k} p_{t_i t_k} \psi_{t_k}^{k \rightarrow i} \prod_{a \in \partial i} \sum_{t_a} q_{t_i t_a} \psi_{t_a}^{a \rightarrow i}, \\
\psi_{t_a}^a &= \beta_{t_a} \frac{e^{-h_{t_a}}}{Z^a} \prod_{j \in \partial a} \sum_{t_j} q_{t_a t_j} \psi_{t_j}^{j \rightarrow a}.
\end{aligned} \tag{6}$$

Based on the marginals obtained using Eq. (6), one can estimate label of each graph node using the one that maximizes the marginal

$$\hat{t}_i = \underset{t}{\operatorname{argmax}} \psi_{t_i}^i. \tag{7}$$

In Bayes inference,  $\hat{t}_i$  is the *maximum posterior estimate*, which gives the optimal results with the minimum mean square error (MMSE) [16]. The essential approximation applied in the belief propagation is the conditional independence assumption, which is exact on trees. Thus BP gives exact posterior marginals if the given graph is a tree, reflecting the fact that the Bethe approximation (3) is always correct in a tree for describing any joint probability distribution. Empirically BP also gives a good approximation to the true posterior marginals if the graph is sparse and have locally tree like structures, hence is widely applied to inference problems in sparse systems [14].

#### IV. DETECTABILITY TRANSITIONS OF JSBM

If the graph is generated by the JSBM, and the parameters  $\theta$  are known, the cavity method provides asymptotically exact analysis; the belief propagation algorithm almost always converges using correct parameters, without encountering the spin glass phase due to the Nishimori line property [15, 16]. Thus, asymptotically exact properties such as phase diagram of the JSBM can be studied directly at the thermodynamic limit by analysing the messages of the belief propagation.

Observe that there is always a trivial fixed point of BP (4)

$$\begin{aligned}
\psi_{t_i}^{i \rightarrow j} &= \psi_{t_i}^{i \rightarrow a} = \psi_{t_i}^i = \alpha_{t_i}, \\
\psi_{t_a}^{a \rightarrow i} &= \psi_{t_a}^a = \beta_{t_a}.
\end{aligned} \tag{8}$$

This fixed point states that every node in the graph has equal probability of belonging to every group, so is known as *paramagnetic fixed point* or *liquid fixed point*. It indicates that the marginals do not provide any information about the ground-true node labels, but only reflect the permutation symmetry of the system. When the paramagnetic fixed point is stable, the system is in the paramagnetic state, we conjecture that no algorithm can find information of the ground-true labels with a success better than a random guess. This conjecture for the stochastic block model is also known as non-detectable phase, its existence has been mathematically proved in [18]. Here we extend this conjecture to the JSBM with both edges and node features. The un-detectable phase in the JSBM has conceptual analogous meaning of the ferromagnetic Ising model in paramagnetic phase where the underlying ground-true labels are the all-one configuration; and analogous to the Hopfield model where the underlying ground-true labels are the stored patterns. From the view point of statistical inference, edges  $\{(ij)\}$  and hyper edges  $\{(ia)\}$  are observations to the signal (i.e. the ground-true labels), so the paramagnetic phase indicates that the number of observations is too few to reveal any information of the signal. An extreme example is that when there is no edge or hyper edge at all, every group assignment for graph node labels has equal probability, hence there is for sure no way to recover any information of the ground true labels using any algorithm.

When the number of observations increases, the paramagnetic fixed point will eventually become unstable, leading to a non-trivial fixed point of belief propagation (4) which are correlated with the ground-true group labels that can be extracted using Eq. (7). The point where the paramagnetic fixed point of belief propagation becomes unstable is the *detectability transition* of the JSBM which puts fundamental limit on ability of all possible algorithms in detecting information of the ground-true labels, and is algorithm independent.

This transition can be determined using the stability analysis of the BP paramagnetic fixed point (8) under random perturbations. Assume that the graph gener-

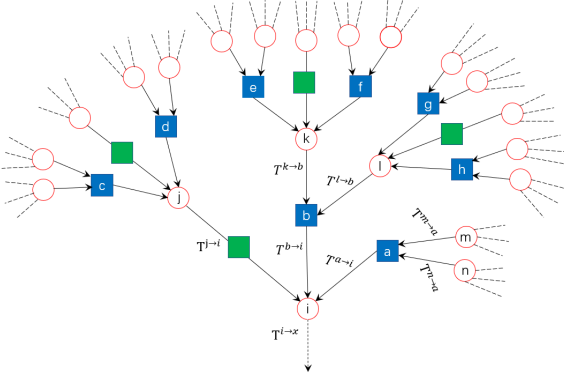


FIG. 2. Illustration of noise propagation from leaves of a tree to the root  $i$ , weighted by eigenvalues of the Jacobian matrices related to BP messages (10). The red circles in the figure denote graph nodes, green circles represent edges connecting graph nodes, and blue boxes represent features, i.e. hyper edges in the factor graph.

ated using the JSBM has  $n \rightarrow \infty$  graph nodes,  $m \rightarrow \infty$  feature nodes. Each graph node is connected to on average  $c_1$  graph nodes and  $c_2$  feature node, and each feature node is connected to on average  $c_3$  graph nodes. Consider putting some random noise with zero mean and unit variance on every node of the graph. Using the locally-tree like property of the graph, after one-step iteration of BP equations (4), noise will be propagated to on average  $c_1$  graph nodes through edges, and  $c_2 c_3$  graph nodes through features (i.e. hyper edges). The process of the noise propagation in the tree-graph is depicted in Fig. 2. If all leaves of the tree are attached with random noises with zero mean and unit variance, after  $l$ -step iterations of BP equations (4) with  $l \rightarrow \infty$ , the total variance of noise on the root node  $i$  can be computed as

$$\mathcal{V} = \lim_{l \rightarrow \infty} (c_1 \lambda_1^2 + c_2 c_3 \lambda_2^4)^l. \quad (9)$$

Where  $c_1$  and  $c_2$  are the average degree of graph nodes and factor nodes respectively, which also equals to the average excess degree when the degree distribution is Poisson as in the JSBM. The details of derivation can be found in the Appendix.  $\lambda_1$  and  $\lambda_2$  are the largest eigenvalue of the Jacobian matrix  $\mathbf{T}^{i \rightarrow j}$  with respect to messages passing from a graph node  $i$  to another graph node  $j$  along edge  $(ij)$ , and the Jacobian matrix  $\mathbf{T}^{a \rightarrow i}$  corresponding to message passing from a feature node  $a$  to a graph node  $i$ , respectively. The elements of the Jacobian matrices (together with the third matrix  $\mathbf{T}^{i \rightarrow a}$ ) evaluated at the paramagnetic fixed point are written as

$$\begin{aligned} T_{t_i t_j}^{i \rightarrow j} &= \frac{\partial \psi_{t_j}^{j \rightarrow x}}{\partial \psi_{t_i}^{i \rightarrow j}} \Big|_{\alpha_{t_i}} = \alpha_{t_i} \left( \frac{np_{t_i t_j}}{c_1} - 1 \right), \\ T_{t_i t_a}^{a \rightarrow i} &= \frac{\partial \psi_{t_i}^{i \rightarrow x}}{\partial \psi_{t_a}^{a \rightarrow i}} \Big|_{\alpha_{t_i}, \beta_{t_a}} = \alpha_{t_i} \left( \frac{mq_{t_i t_a}}{c_2} - 1 \right), \\ T_{t_a t_i}^{i \rightarrow a} &= \frac{\partial \psi_{t_a}^{a \rightarrow j}}{\partial \psi_{t_i}^{i \rightarrow a}} \Big|_{\alpha_{t_i}, \beta_{t_a}} = \beta_{t_a} \left( \frac{mq_{t_a t_i}}{c_2} - 1 \right). \end{aligned} \quad (10)$$

The paramagnetic fixed point is unstable under random perturbation whenever  $\mathcal{V} > 1$ , it indicates that the detectability phase transition locates at

$$c_1 \lambda_1^2 + c_2 c_3 \lambda_2^4 = 1. \quad (11)$$

This kind of stability condition is also known in the spin glass literature as the Almeida-Thouless local stability condition [19], and in the computer science as the Kesten-Stigum bound on reconstruction on trees [20, 21], and robust reconstruction threshold [22].

To clearly illustrate the phase transitions and phase diagrams we use a simple case of diagonal  $\mathbf{P}$  matrix with  $p_{\text{in}}$  on the diagonal and  $p_{\text{out}}$  on the off-diagonal elements, and diagonal  $\mathbf{Q}$  matrix with  $q_{\text{in}}$  on the diagonal and  $q_{\text{out}}$  on the off-diagonal. We notice that there are constraints on the matrix elements

$$\begin{aligned} p_{\text{in}} + (\kappa - 1)p_{\text{out}} &= \frac{\kappa c_1}{n}, \\ q_{\text{in}} + (\kappa - 1)q_{\text{out}} &= \frac{\kappa c_2}{m}, \end{aligned} \quad (12)$$

which means that there is only one free parameter for each matrix. So we introduce parameters  $\epsilon_1 = \frac{p_{\text{in}}}{p_{\text{out}}}$  and  $\epsilon_2 = \frac{q_{\text{in}}}{q_{\text{out}}}$  for parametrizations. In this setting, we have a simpler expression for eigenvalues

$$\lambda_1 = \frac{1 - \epsilon_1}{1 + \epsilon_1} \quad \lambda_2 = \frac{1 - \epsilon_2}{1 + \epsilon_2}. \quad (13)$$

To verify our theoretical results on the detectability transitions, we carry out numerical experiments on large synthetic graphs generated by the JSBM, and compare the results obtained by the belief propagation with theoretical predictions. The accuracy of belief propagation are evaluated using overlap between the obtained partition  $\{\hat{t}_i\}$  and the ground-truth partition  $\{t_i^*\}$

$$\mathcal{O}(\{\hat{t}_i\}, \{t_i^*\}) = \max_{\pi} \frac{1}{n} \sum_{i=1}^n \delta(\pi_{\hat{t}_i}, t_i^*), \quad (14)$$

which is computed by maximizing over all  $\kappa!$  permutations of  $\kappa$  groups  $\pi$ . We can see from the definition Eq. (14) that if the inferred labels  $\{\hat{t}_i\}$  is randomly chosen which has nothing to do with the ground-truth one  $\{t_i^*\}$ , the overlap would be  $1/\kappa$ ; otherwise if the inferred label is correlated with the ground-truth, the overlap  $\mathcal{O}(\{\hat{t}_i\}, \{t_i^*\})$  will be greater than  $1/\kappa$  and is upper-bounded by 1.0 which indicates an exact match of two

labels. Overlap is a commonly chosen quantity for estimating similarity between two group assignments with a small number of groups. When the number of groups is large, or with different group sizes, we should use other measures such as normalized mutual information and its variances [23, 24].

The BP overlaps are shown in Fig. 3. In the left panel of the figure we fix  $\epsilon_2 = 0.3$ , and plot the overlap obtained by belief propagation with varying  $\epsilon_1$ . In the middle panel,  $\epsilon_1$  is fixed to 0.3 and  $\epsilon_2$  varies. We can see from the figure that the overlap is always quite close to 1.0 with a small  $\epsilon$  values indicating that the reconstruction of ground-truth is almost perfect. With  $\epsilon$  increases, the accuracy of inference decreases, and eventually goes to 0.5. The point that the overlap decays to 0.5 coincides very well with the prediction of the detectability transition (11) which is indicated by the dashed lines. With  $\epsilon_1$  and  $\epsilon_2$  beyond the detectability transition, system is in the paramagnetic phase, and BP overlap is always 0.5 which is identical to the accuracy of random guess in two groups. We also claim that the overlap obtained by BP, those are the lines indicated in the figure, are optimal among all possible algorithms in the thermodynamic limit. In the right panel of Fig. 3 we report accuracy of belief propagation on the  $\epsilon_1$ - $\epsilon_2$  plane where the overlap decays from a large value to non-informative 0.5 (indicated by the colors). The magenta dashed line represents theoretical predictions of the phase transition given by (11), which matches very well with the numerical experiments.

## V. FROM BELIEF PROPAGATION TO GRAPH CONVOLUTION NETWORK

When applying the previously introduced BP algorithm to real-world graphs or to synthetic graph without knowing the parameters, an essential problem is how to learn parameters  $\theta$ . A classic approach is the Expectation Maximization (EM) [25], which updates parameters by maximizing the total log-likelihood of data, that is, minimizing the total free energy in the language of physics. However, in practice the EM for minimizing free energy is prone to overfitting [11] and suffers from trapping into local minimal of free energy. Note that in the setting of semi-supervised learning, we have a small amount of labels, thus the parameters learning can be done in the supervised fashion by matching predicted labels and training labels. We propose to first expand and truncate the belief propagation equations to finite time steps as a forward step, then learn the JSBM parameters  $\theta$  using back-propagation. We call the algorithm *Belief Propagation Graph Convolution Network (BPGCN)*, as the whole procedure is analogous to the canonical graph convolution networks [1], but with a different convolution kernel and non-linear activation functions that come from the mathematically principled message passing equations for optimal JSBM inference. In this sense, the param-

eters of the JSBM  $\mathbf{P}$  and  $\mathbf{Q}$  become weight matrices of the neural network to be learnt. The input of the network is a randomly initialized cavity messages (at 0-th layer)  $\Psi_0^{i \rightarrow j} \in \mathbb{R}^{2M_1 \times \kappa}$ ,  $\Psi_0^{i \rightarrow a} \in \mathbb{R}^{2M_2 \times \kappa}$  and  $\Psi_0^{a \rightarrow i} \in \mathbb{R}^{2M_2 \times \kappa}$ , and marginal matrix  $\Psi_0^i \in \mathbb{R}^{n \times \kappa}$  and  $\Psi_0^a \in \mathbb{R}^{m \times \kappa}$ , where  $M_1$  and  $M_2$  are number of edges in uni-partite graph and bi-partite graph. The forward pass of the network naturally comes from the iterative equations of BP, and the propagation equation from the  $l$ -th layer to the  $l+1$ -th layer are formulated as

$$\begin{aligned} \Psi_{l+1}^a &= \text{Softmax} \left[ \mathbf{E} \log(\Psi_l^{i \rightarrow a} \mathbf{P}) \right] \\ \Psi_{l+1}^i &= \text{Softmax} \left[ \mathbf{H} \log(\Psi_l^{a \rightarrow i} \mathbf{Q}) + \mathbf{C} \log(\Psi_l^{i \rightarrow j} \mathbf{P}) \right] \\ \Psi_{l+1}^{i \rightarrow j} &= \text{Softmax} \left[ \mathbf{N} \log(\Psi_l^{a \rightarrow i} \mathbf{Q}) + \mathbf{B} \log(\Psi_l^{i \rightarrow j} \mathbf{P}) \right] \\ \Psi_{l+1}^{i \rightarrow a} &= \text{Softmax} \left[ \mathbf{M} \log(\Psi_l^{i \rightarrow j} \mathbf{P}) + \mathbf{R} \log(\Psi_l^{a \rightarrow i} \mathbf{Q}) \right] \\ \Psi_{l+1}^{a \rightarrow i} &= \text{Softmax} \left[ \mathbf{D} \log(\Psi_l^{i \rightarrow a} \mathbf{P}) \right] \end{aligned} \quad (15)$$

where the activation function  $\text{Softmax}(z_t) = \frac{e^{z_t}}{\sum_{s=1}^{\kappa} e^{z_s}}$  is inherited from BP which asks to normalize various marginal probabilities with  $\kappa$  components. If  $\kappa = 2$ , the Softmax activation function reduces to the sigmoid function. Matrices  $\mathbf{E}, \mathbf{H}, \mathbf{C}, \mathbf{N}, \mathbf{B}, \mathbf{M}, \mathbf{R}, \mathbf{D}$  are non-backtracking matrices [26] encoding adjacent information of cavity messages. The detailed explanations of forward propagation of the BPGCN can be found at the Appendices.

Assume that the depth of the BPGCN is  $L$ , then the marginals of graph nodes  $\Psi = \{\Psi_L^i\} \in [0, 1]^{n \times \kappa}$  is the output of BPGCN. After that, we choose a loss function on the training labels (a small fraction of known labels in the semi-supervised learning). A common choice of loss function for classifications is the cross entropy, which is defined as

$$\mathcal{L} = - \sum_{i \in \Omega} \sum_{s=1}^{\kappa} \mathbf{y}_i s \ln \psi_L^i s \quad (16)$$

where  $\Omega$  denotes the (training) set of graph nodes,  $\mathbf{y}_i$  stands for the labels for node  $i$  in the training set, with  $\mathbf{y}_i = \{y_{is}\} = \{0, 0, \dots, 1, \dots, 0\}$  being the one-hot vector.

The training of the NBGCN is the same as other graph convolution networks: in each epoch (loop) of training we first do a forward pass and evaluate the cross entropy loss function on the training set, then use the *Back Propagation* [2] algorithm to compute the gradients of the loss function with respect to elements in  $\mathbf{P}$  and  $\mathbf{Q}$  matrices, then apply (stochastic) gradient descent or its variants (such as ADAM [27]) to update parameters. We note here that the final evaluation of the algorithm is the accuracy of the predicted labels on the nodes with unknown labels in the test set.

The crucial difference between BPGCN and belief propagation (BP) (including the semi-supervised version [12]) is that BP minimizes the Bethe free energy, while BPGCN minimizes the loss function evaluated on

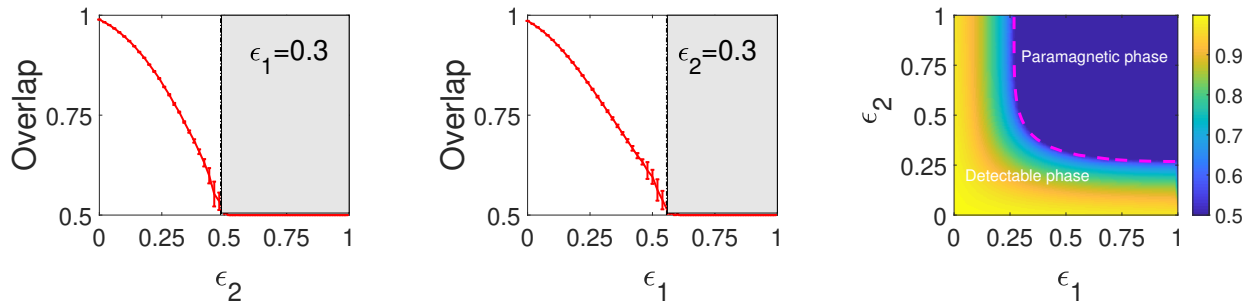


FIG. 3. Overlap as a function of  $\epsilon_1$  and  $\epsilon_2$ , all networks are generated with  $n = 2 * 10^5, m = 2 * 10^5$ , group numbers  $\kappa = 2$ , and average degree  $c_1 = c_2 = 3$ . On the left panel,  $\epsilon_2$  is fixed to 0.3; on the middle panel,  $\epsilon_1$  is fixed to 0.3; the detectability threshold agrees with the theoretical calculations(11) except for fluctuations because of finite size effect. On the right panel, overlap as a function of  $\epsilon_1$  and  $\epsilon_2$  is plotted, the magenta dashed line shows the detectability threshold calculated using (11).

the training data. On large JSBM synthetic graphs, free energy is the best loss function to minimize. However when applied on graphs that were not generated by JSBM, minimizing Bethe free energy or energy is prone to overfitting [11, 28]. Moreover, in BPGCN the adaptive fields Eq. (5), that contributed by non-edges in BP, are not necessary, because the labels automatically balance the group sizes. There are two main differences between BPGCN and the standard graph neural networks: First, the activation function in BPGCN is determined by BP message passing equations rather than being chosen manually. This is in contrast with usual graph convolution networks where many activation functions such as ReLU, PReLU and Tanh are available under choice. Second, there are only few trainable parameters in BPGCN, which are elements of  $\mathbf{P}$  and  $\mathbf{Q}$  matrices. They are totally shared across all layers of the neural network. This certainly limits the overall representation power of the BPGCN, but could in principle enhances very much the generalization power of the model. Indeed, in the semi-supervised classifications, the amount of training data is much fewer than in the normal supervised setting, and the number of observations is proportional to the number of edges (and hyper edges), so the totally shared parameters are very helpful in preventing overfitting the training data.

## VI. COMPARING BPGCN WITH OTHER GRAPH CONVOLUTION NETWORKS

In this section we compare the performance of our BP and BPGCN with several state-of-the-art graph convolution networks on various datasets. These algorithms we compare with include

### 1. Graph Convolution Network (GCN) [1]

GCN is probably the most famous graph convolution network which drastically outperformed all non-neural-network type algorithms when it was proposed in 2017. The layer-wise forward propagation rule of the GCN is

formulated as

$$\mathbf{H}^{(l+1)} = \text{ReLU}\left(\tilde{\mathbf{A}}\mathbf{H}^{(l)}\mathbf{W}^{(l)}\right), \quad (17)$$

where  $\mathbf{H}^{(l)}$  and  $\mathbf{W}^{(l)}$  are states of hidden variables and weight matrix at the  $l$ -th layer respectively,  $\tilde{\mathbf{A}}$  is the graph convolution kernel, which is defined as

$$\tilde{\mathbf{A}} = \mathbf{D}^{-\frac{1}{2}}(\mathbf{A} + \mathbf{I})\mathbf{D}^{-\frac{1}{2}}, \quad (18)$$

with  $\mathbf{D}$  being a diagonal degree matrix with  $D_{ii} = 1 + \sum_k A_{ik}$ . The propagation rule of the GCN was motivated by a first-order approximation of localized spectral filters, we will discuss in detail in the Appendices. Therefore a standard two layers GCN can be written as:

$$\mathbf{Z} = \text{Softmax}[\tilde{\mathbf{A}}\text{Relu}(\tilde{\mathbf{A}}\mathbf{F}\mathbf{W}^0)\mathbf{W}^1], \quad (19)$$

where  $\mathbf{Z} \in \mathbb{R}^{n \times \kappa}$  is the predictions.

### 2. Approximate Personalized Propagation of Neural Predictions (APPNP) [3]

Similar to the GCN, APPNP extract feature information (which is encoded in the  $\mathbf{F}$ ) to hidden neuron states using a multi-layer perceptron (MLP)

$$\mathbf{H} = \text{MLP}(\mathbf{F})$$

then propagate the hidden states  $\mathbf{H}$  via personalized PageRank scheme to produce predictions of node labels.

$$\begin{aligned} \mathbf{Z}^{(k+1)} &= (1 - \omega)\tilde{\mathbf{A}}\mathbf{Z}^{(k)} + \omega\mathbf{H} \\ \mathbf{Z} &= \text{Softmax}[(1 - \omega)\tilde{\mathbf{A}}\mathbf{Z}^{(K-1)} + \omega\mathbf{H}], \end{aligned} \quad (20)$$

In the recent benchmarking studies on performance of popular GCNs, APPNP performs the best among various of datasets [29].

### 3. Graph attention network (GAT) [4]

The GAT adopts the fashion and complex *attention mechanism* [30] to learn attention coefficients (weights) between pair of connected nodes. This can be seen as based on adjacency matrix but with learned adjustable weights on the edges.

#### 4. Simplified Graph Convolution Networks (SGCN) [31]

The SGCN tries to remove redundant and unnecessary computations from popular graph convolution networks, resulting into a simple low-pass filter followed by a linear classifier. Finally the SGCN takes a simple propagation rule using  $k$ -th power of the variant adjacency matrix  $\tilde{\mathbf{A}}$  as in GCN:

$$\mathbf{Z} = \text{Softmax}(\tilde{\mathbf{A}}^k \mathbf{F}\mathbf{W}) \quad (21)$$

The empirical results show that the simplification captures the essential reasons for success of GCNs, giving positive impact on accuracy as well as speed up over GCNs.

#### A. Comparisons on synthetic datasets

We first compare algorithms on synthetic networks generated by the JSBM. In the experiments we give a fraction  $\rho = 0.05$  randomly chosen node labels as supervision. Also, like usual experimental setup in the studies of classifications, we randomly choose 500 nodes with known labels as validation sets for tuning network hyper-parameters and early stopping strategy in order to get better generalizations on the test set. The classification accuracy is evaluated using the overlap (14) on the rest of the node (test set) labels. Here, We choose a very straightforward (although not optimal) initial  $\mathbf{P}$  matrix in BPGCN which contains two kinds of elements,  $p_{\text{in}}$  on the diagonal and  $p_{\text{out}}$  on the off-diagonal, with ratio  $\epsilon_1 = p_{\text{out}}/p_{\text{in}}$ . The  $\mathbf{Q}$  matrix is initialized in a similar way with  $\epsilon_2 = q_{\text{out}}/q_{\text{in}}$ . For all synthetic networks, we use  $\epsilon_1 = \epsilon_2 = 0.5$  as initial conditions for NBGCN. Notice that for sure we can tune the initial  $\epsilon_1$  and  $\epsilon_2$  with validation sets on every synthetic network to obtain better generalization on test dataset but in this study we have not done this.

We have carried out extensive numerical experiments on large synthetic graphs with varying average degrees and varying signal-to-noise ratio  $\epsilon$ . Most of the results are plotted in the Appendices, and representative results are shown in Fig. 4. The first message follows from our results is that the BPGCN performs very close to the asymptotically optimal BP results, but all other GCNs do not. In the left panel of the figure,  $c_1$  is fixed to 4, and  $c_2$  increases from 3 to 20. We can see that GCN, APPNP, GAT, and SGCN work much worse than BPGCN, even when  $c_2$  is quite large. In the middle panel of the graph, we fix  $c_2$  to 4 and vary  $c_1$ . The figure demonstrates that when  $c_1$  is small, GCN, APPNP, GAT, and SGCN perform poorly, which is consistent with what the left panel shows. This observation gives a clear evidence that existing popular graph convolution networks are significantly more influenced by the sparsity in the graph structure. We call the issue of conventional GCNs *sparsity issue*.

In the right panel in Fig. 4, we compare performance of GCNs with  $\epsilon_2$  fixed to 0.1, average degrees fixed to  $c_1 = 10$ , and  $c_2 = 10$ , and varying  $\epsilon_1$ . We can see

from the figure that while BPGCN works perfectly in the whole range of  $\epsilon_1$ , conventional GCNs fail surprisingly, even when BPGCN gives almost exact results with overlap close to 1.0. This observation indicates that the conventional GCNs we have tested have difficulties in extracting information about group labels contained in the features when the edges of the graph are noisy. Further check on the output of the conventional GCNs show that they all have good training overlap, but have bad test overlap, so this is a clear sign of overfitting to the training labels and noise in the graph edges, which we call *overfitting issue*. In what follows we give analysis on these two issues and give suggestions on how to overcome them based on features of BPGCN which is immune to the issues.

*Sparsity issue:* Properties of the forward-propagation of GCNs are closely related to linear convolution kernels used by the GCNs, so the reason for the sparsity issue can be understood by studying the spectrum of the linear convolution kernel used in graph convolutions. In the GCN, SGCN and APPNP, the linear convolution kernel is the variant of the normalized adjacency matrix  $\tilde{\mathbf{A}}$  (18). It has been established in e.g. [26, 32] that this kind of linear operators have localization problems in large sparse graphs, with leading eigenvectors encoding only local structures, rather than global information of labels. In the appendices we gave a detailed analysis on the spectral localization problem of conventional convolution filters. In the contrast, our approach, BPGCN, is immune to the sparsity issue, because the linear convolution kernel of the BPGCN is the non-backtracking matrix, which naturally works well and overcome the localization problems in the large sparse networks [26]. Thus, a straight forward way of overcoming the sparsity issue in the classic GCNs might be considering using a linear kernel that does not have the localization problems in the sparse graphs, such as the non-backtracking matrix, or the X-Laplacian [32].

*Overfitting issue:* From Eq. (17), Eq. (20) and Eq. (21) we observe that for the linear filters are always directly operate on the weight matrix, or hidden states. This reflects a straightforward assumptions in the conventional GCNs: the relational data, i.e. edges or adjacency matrix of the graph, must contain information of the labels. This is a natural assumption, but should not be always true. In contrast, the BPGCN overcomes this defects by learning an affinity matrix  $\mathbf{P}$  which stores essentially the learned signal-to-noise ratio corresponding to the edges, which may identify that there is no information encoded in graph edges. Based on this observation, a simple solution would be applying an affinity matrix to the convolution kernel in conventional GCNs, just as what NBGCN does



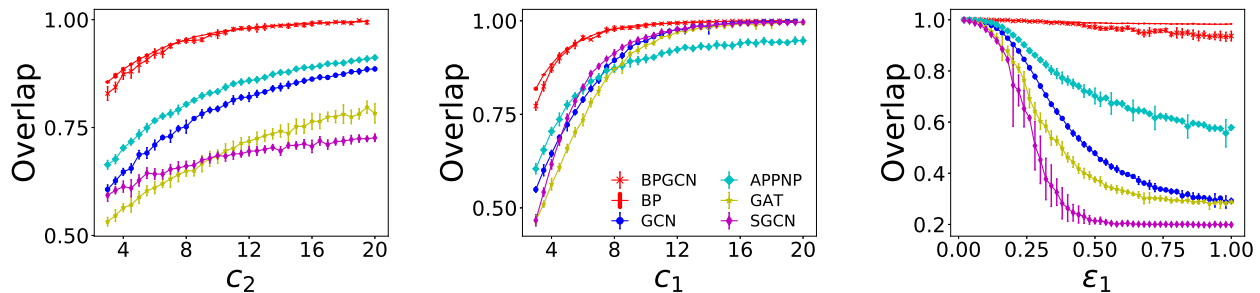


FIG. 4. Overlap comparisons between BP, BPGCN and conventional GCNs on synthetic networks generated by the JSBM with varying parameters. In all experiments, each generated graph has  $n = 10,000$  nodes,  $m = 10,000$  features,  $\kappa = 5$  groups; a fraction of 0.05 nodes are selected randomly in training set with known labels, and the validation set also contains 0.05 fraction of nodes, with rest of nodes belonging to the test set on which the overlaps (14) are evaluated. Each data point in the figure is averaged over 10 instances. (Left)  $\epsilon_1 = 0.1$ ,  $\epsilon_2 = 0.2$ , and  $c_1 = 4$ , with vary  $c_2$ ; (Middle)  $\epsilon_1 = 0.1$ ,  $\epsilon_2 = 0.2$ , and  $c_2 = 4$ , and  $c_1$  is varying; (Right)  $c_1 = c_2 = 10$ ,  $\epsilon_2$  is fixed to 0.2, and  $\epsilon_1$  ranges from 0 to 1.

## B. Comparisons on real-world datasets

Next we apply the BPGCN on several commonly used real-world networks with and without node features. The KARATE CLUB network [33] and POLITICAL BLOGS network [34] are classic networks containing community structures. In these two networks there are no node features, canonical GCNs usually use identity matrix as feature matrix [1]. In the KARATE CLUB network we use 2 labels per group as training labels, and 2 labels per group as validate labels. In the POLITICAL BLOGS network we use 10 labels per group as training labels and 10 labels per group as validation set. The CITESEER, CORA and PUBMED networks are standard datasets for semi-supervised classifications used in almost all studies related to graph neural networks. We follow exactly the same split of training, test and validation set as in [1] on these graphs. In these networks, there are *ground true* labels for each node coming from expert division (in KARATE CLUB and POLITICAL BLOGS) or from human analysis of content of each article (such as research area of articles in citation networks). Labels of both training and validation sets are visible to GCN algorithms, the task of GCN algorithms is to predict labels of the unseen test set. The performance of the algorithms are evaluated using the overlap between predictions and the ground-true labels on the test set.

In the BPGCN algorithm, we use a tunable external field as hyper parameter to adjust the strength of the training label acting on the node. We also did a simple search for hyperparameters including external field strength, network layers using validation set. We again choose a very straightforward (although not optimal) initial  $\mathbf{P}$  matrix in BPGCN which contains two kinds of elements,  $p_{\text{in}}$  on the diagonal and  $p_{\text{out}}$  on the off-diagonal, with ratio  $\epsilon_1 = p_{\text{out}}/p_{\text{in}}$ . The  $\mathbf{Q}$  matrix is initialized similarly with  $\epsilon_2 = q_{\text{out}}/q_{\text{in}}$ . In contrast to synthetic network, we did a simple search for  $\epsilon_1$  and  $\epsilon_2$  using validation set. The details of parameters as well as hyper parameters

can be found at the appendices.

Our comparison results are listed in the Table I. We can see from the table that on the two networks without node features, KARATE CLUB network and the POLITICAL BLOGS network, all GCNs performs quite well, indicating that all of them have succeeded in extracting labeling information from edges of the network. Our algorithm, BPGCN, outperforms other three GCNs in the POLICAL BLOGS networks. We think the good performance comes from the non-backtracking convolution kernel, which is known to give good spectral properties on the large sparse graphs such as POLITICAL BLOGS network [26].

On three networks with node features, CITESEER, CORA, and PUBMED, we see different quantitative behaviors. On CITESEER and CORA, the BPGCN performs comparably to other GCNs. Particularly, on the CITESEER network, our algorithm outperforms Graph Attention Network, and on the CORA network, BPGCN outperforms Graph Convolution Networks. However, the BPGCN works poorly on the PUBMED network, giving the worse performance among all GCNs. The reason is that the PUBMED network contains 19717 nodes, but only 500 features. This means that the features are densely connected to nodes so the bipartite part of the graph significantly deviates from sparse random graphs where the JSBM model and our BPGCN algorithm rely on. As a consequence, our algorithm is not able to extract the information from the features very well. Indeed, we have verified that by completely ignoring the features, our algorithm gives even better classification accuracy 70.1% using only the edges of the graph. We also noticed that the Multilayer perceptron (MLP) which uses only the information of the features already achieves an high accuracy. So a simple remedy to the BPGCN in the situation that the feature (the bipartite part of the graph) is far from locally-tree-like structures, we simply take the results given by MLP instead of using the bipartite graph, as an external field acting on the BPGCN. We confirm that this strategy lifts the accuracy of BPGCN on the

PUBMED network to 80.1%, which is as good as the state-of-the-art results given by the APPNP.

	KARATE	POLBLOGS	CITeseer	CORA	PUBMED
# nodes	34	1490	3327	2078	19717
# features	0	0	3703	1433	500
$c$	4.6	22.4	2.78	3.89	4.49
MLP [1]	—	—	58.4	52.2	72.7
GCN [1]	<b>96.5</b>	86.2	71.1	81.5	79.0
GAT [4]	87.9	88.7	70.8	83.1	78.5
SGCN [31]	91.6	81.3	71.3	81.7	78.9
APPNP [3]	96.3	87.5	<b>71.8</b>	<b>83.5</b>	<b>80.1</b>
BPGCN	95.8	<b>89.3</b>	71.1	82.1	70.0

TABLE I. Comparison of classification accuracy on test set of real-world graphs. Results of GCNs on CORA, PUBMED and CITeseer are copied from benchmarking results in [29]. In the table,  $c$  is the average degree of the graph, KARATE denotes Zakary’s Karate Club network [35], and POLBLOGS denotes the Political Blogs network [36]. Results of GCNs on the Karate Club network Political Blogs network are evaluated using publically available implementations of each GCN.

## VII. CONCLUSIONS AND DISCUSSIONS

We have proposed to model semisupervised classification in graphs with both pairwise relational features and node features using the joint stochastic block model. We gave a theoretical analysis on the detectability transition and phase diagram, using the cavity method in the statistical physics and the belief propagation algorithm which we claim to be asymptotically exact in the thermodynamic limit. The JSBM can be used to generate benchmark networks with continuously tunable parameters, asymptotically optimal algorithms and accuracy. The benchmarks are particularly useful in evaluating graph

neural networks with different design arts. In particular, we found that the state-of-the-art graph convolution networks we have tested all perform poorly in sparse graphs, which we can understand using spectral properties of the convolution kernels in the GCNs. We also observe that popular GCNs tends to overfit the training labels when the edges in the graph carry few information about group labels.

Our algorithm naturally translates to a graph convolution network, BPGCN. In contrast to the popular graph convolution networks, the convolution kernel and activation function are determined mathematically from Bayesian optimal inference algorithm of the JSBM. We show that on synthetic networks our algorithm greatly outperforms existing graph convolution networks, and gives high classification accuracy in the parameter regime that conventional GCNs fail to work. On the real-world networks our algorithm also displays comparable performance to the state-of-the art GCNs in most cases.

The BPGCN has a unique feature that it is quite powerful in extracting label information from edges of the graph, and significantly outperforms existing GCNs we have tested on this point. This power comes from the non-backtracking convolution kernel inherited from the belief propagation algorithm. The weakness of the BPGCN is also illustrated using the Pubmed dataset in which the features is too extensive to be approximated by a random bipartite graph. We give a simple remedy to replace the bipartite graph by external field given by a multi layer perceptron. Based on the fact that the BPGCN is immune to the sparsity issue and overfitting issue of conventional GCNs, we have discussed how to improve current GCN techniques. It would be interesting to combine the strenghts of BPGCN and state-of-the art GCNs more deeply, which may inspire a new architecture of graph neural networks. We leave this for future work.

- 
- [1] T. N. Kipf and M. Welling, in *International Conference on Learning Representations* (2017).
- [2] I. Goodfellow, Y. Bengio, A. Courville, and Y. Bengio, *Deep learning*, Vol. 1 (MIT press Cambridge, 2016).
- [3] J. Klicpera, A. Bojchevski, and S. Gnnemann, in *International Conference on Learning Representations* (2019).
- [4] P. Velickovi, G. Cucurull, A. Casanova, A. Romero, P. Li, and Y. Bengio, in *International Conference on Learning Representations* (2018).
- [5] J. Gilmer, S. S. Schoenholz, P. F. Riley, O. Vinyals, and G. E. Dahl, in *Proceedings of the 34th International Conference on Machine Learning-Volume 70* (2017) pp. 1263–1272.
- [6] P. W. Battaglia, J. B. Hamrick, V. Bapst, A. Sanchez-Gonzalez, V. Zambaldi, M. Malinowski, A. Tacchetti, D. Raposo, A. Santoro, R. Faulkner, *et al.*, arXiv preprint arXiv:1806.01261 (2018).
- [7] P. W. Holland, K. B. Laskey, and S. Leinhardt, *Social networks* **5**, 109 (1983).
- [8] D. Hric, T. P. Peixoto, and S. Fortunato, *Physical Review X* **6**, 031038 (2016).
- [9] L. Florescu and W. Perkins, in *Conference on Learning Theory* (2016) pp. 943–959.
- [10] J. S. Yedidia, W. T. Freeman, and Y. Weiss, *Exploring artificial intelligence in the new millennium* **8**, 236 (2003).
- [11] A. Decelle, F. Krzakala, C. Moore, and L. Zdeborová, *Physical Review E* **84**, 066106 (2011).
- [12] P. Zhang, C. Moore, and L. Zdeborová, *Physical Review E* **90**, 052802 (2014).
- [13] S. Osindero and G. E. Hinton, in *Advances in neural information processing systems* (2008) pp. 1121–1128.
- [14] M. Mezard and A. Montanari, *Information, Physics and Computation* (Oxford University press, 2009).
- [15] H. Nishimori, *Journal of Physics C: Solid State Physics* **13**, 4071 (1980).
- [16] Y. Iba, *Journal of Physics A: Mathematical and General*

- 32**, 3875 (1999).
- [17] H. Bethe, Proc. R. Soc. London A **150**, 552 (1935).
- [18] E. Mossel, J. Neeman, and A. Sly, *Combinatorica* **38**, 665 (2018).
- [19] J. De Almeida and D. J. Thouless, *Journal of Physics A: Mathematical and General* **11**, 983 (1978).
- [20] H. Kesten and B. P. Stigum, *The Annals of Mathematical Statistics* **37**, 1463 (1966).
- [21] H. Kesten and B. P. Stigum, *Journal of Mathematical Analysis and Applications* **17**, 309 (1967).
- [22] S. Janson, E. Mossel, *et al.*, *The Annals of Probability* **32**, 2630 (2004).
- [23] L. Danon, A. Diaz-Guilera, J. Duch, and A. Arenas, *Journal of Statistical Mechanics: Theory and Experiment* **2005**, P09008 (2005).
- [24] P. Zhang, *Journal of Statistical Mechanics: Theory and Experiment* **2015**, P11006 (2015).
- [25] A. P. Dempster, N. M. Laird, and D. B. Rubin, *Journal of the Royal Statistical Society: Series B (Methodological)* **39**, 1 (1977).
- [26] F. Krzakala, C. Moore, E. Mossel, J. Neeman, A. Sly, L. Zdeborová, and P. Zhang, *Proceedings of the National Academy of Sciences* **110**, 20935 (2013).
- [27] D. P. Kingma and J. Ba, in *International Conference on Learning Representations* (2015).
- [28] P. Zhang and C. Moore, *Proceedings of the National Academy of Sciences* **111**, 18144 (2014).
- [29] M. Fey and J. E. Lenssen, in *ICLR Workshop on Representation Learning on Graphs and Manifolds* (2019).
- [30] A. Vaswani, N. Shazeer, N. Parmar, J. Uszkoreit, L. Jones, A. N. Gomez, L. Kaiser, and I. Polosukhin, in *Advances in neural information processing systems* (2017) pp. 5998–6008.
- [31] F. Wu, A. Souza, T. Zhang, C. Fifty, T. Yu, and K. Weinberger, in *Proceedings of the 36th International Conference on Machine Learning*, Vol. 97 (PMLR, 2019) pp. 6861–6871.
- [32] P. Zhang, in *Advances In Neural Information Processing Systems* (Curran Associates, Inc., 2016) pp. 541–549.
- [33] W. W. Zachary, *Journal of anthropological research* **33**, 452 (1977).
- [34] L. A. Adamic and N. Glance, in *Proceedings of the 3rd international workshop on Link discovery* (ACM, 2005) pp. 36–43.
- [35] W. W. Zachary, *Journal of anthropological research* , 452 (1977).
- [36] L. A. Adamic and N. Glance, in *Proceedings of the 3rd international workshop on Link discovery* (ACM, 2005) pp. 36–43.
- [37] Y. LeCun, Y. Bengio, *et al.*, *The handbook of brain theory and neural networks* **3361**, 1995 (1995).
- [38] A. Krizhevsky, I. Sutskever, and G. E. Hinton, in *Advances in neural information processing systems* (2012) pp. 1097–1105.
- [39] J. Bruna, W. Zaremba, A. Szlam, and Y. LeCun, in *2nd International Conference on Learning Representations* (2014).
- [40] D. K. Hammond, P. Vandergheynst, and R. Gribonval, *Applied and Computational Harmonic Analysis* **30**, 129 (2011).
- [41] J. Weston, F. Ratle, H. Mobahi, and R. Collobert, in *Neural Networks: Tricks of the Trade* (Springer, 2012) pp. 639–655.
- [42] Z. Yang, W. W. Cohen, and R. Salakhutdinov, in *Proceedings of the 33rd International Conference on International Conference on Machine Learning-Volume 48* (JMLR. org, 2016) pp. 40–48.
- [43] X. Zhu, Z. Ghahramani, and J. D. Lafferty, in *Proceedings of the 20th International conference on Machine learning (ICML-03)* (2003) pp. 912–919.
- [44] B. Perozzi, R. Al-Rfou, and S. Skiena, in *Proceedings of the 20th ACM SIGKDD international conference on Knowledge discovery and data mining* (ACM, 2014) pp. 701–710.
- [45] Q. Lu and L. Getoor, in *Proceedings of the 20th International Conference on Machine Learning (ICML-03)* (2003) pp. 496–503.

## Appendix A: Deriving belief propagations

Starting from the Boltzmann distribution Eq. (1), and definition of likelihood function Eq. (2), using the variational distribution with form Eq. (3), by minimizing the Bethe free energy with respect to constraint subject to normalizations of marginals, we can arrive at the standard form of belief propagation [10] for the JSBM:

$$\begin{aligned}
\psi_{t_i}^{i \rightarrow j} &= \frac{\alpha_{t_i}}{Z^{i \rightarrow j}} \prod_{k \in \partial i \setminus j} \sum_{t_k} p_{t_i t_k} \psi_{t_k}^{k \rightarrow i} \prod_{k \notin \partial i \setminus j} \sum_{t_k} (1 - p_{t_i t_k}) \psi_{t_k}^{k \rightarrow i} \cdot \prod_{a \in \partial i} \sum_{t_a} q_{t_i t_a} \psi_{t_a}^{a \rightarrow i} \prod_{a \notin \partial i} \sum_{t_a} (1 - q_{t_i t_a}) \psi_{t_a}^{a \rightarrow i} \\
\psi_{t_i}^{i \rightarrow a} &= \frac{\alpha_{t_i}}{Z^{i \rightarrow a}} \prod_{k \in \partial i} \sum_{t_k} p_{t_i t_k} \psi_{t_k}^{k \rightarrow i} \prod_{k \notin \partial i} \sum_{t_k} (1 - p_{t_i t_k}) \psi_{t_k}^{k \rightarrow i} \cdot \prod_{b \in \partial i \setminus a} \sum_{t_b} q_{t_i t_b} \psi_{t_b}^{b \rightarrow i} \prod_{b \notin \partial i \setminus a} \sum_{t_b} (1 - q_{t_i t_b}) \psi_{t_b}^{b \rightarrow i} \\
\psi_{t_a}^{a \rightarrow i} &= \frac{\beta_{t_a}}{Z^{a \rightarrow i}} \prod_{j \notin \partial a \setminus i} \sum_{t_j} q_{t_a t_j} \psi_{t_j}^{j \rightarrow a} \prod_{j \in \partial a \setminus i} \sum_{t_j} (1 - q_{t_a t_j}) \psi_{t_j}^{j \rightarrow a}.
\end{aligned} \tag{A1}$$

where  $\psi_{t_i}^{i \rightarrow j}$ ,  $\psi_{t_i}^{i \rightarrow a}$ , and  $\psi_{t_a}^{a \rightarrow i}$  are cavity probabilities as we have stated in the main text. The marginal probabilities are estimated as a function of cavity probabilities

as

$$\begin{aligned}
\psi_{t_i}^i &= \frac{\alpha_{t_i}}{Z^{i \rightarrow j}} \prod_{k \in \partial i} \sum_{t_k} p_{t_i t_k} \psi_{t_k}^{k \rightarrow i} \prod_{k \notin \partial i} \sum_{t_k} (1 - p_{t_i t_k}) \psi_{t_k}^{k \rightarrow i} \\
&\cdot \prod_{a \in \partial i} \sum_{t_a} q_{t_i t_a} \psi_{t_a}^{a \rightarrow i} \prod_{a \notin \partial i} \sum_{t_a} (1 - q_{t_i t_a}) \psi_{t_a}^{a \rightarrow i} \\
\psi_{t_a}^a &= \frac{\beta_{t_a}}{Z^{a \rightarrow i}} \prod_{j \notin \partial a} \sum_{t_j} q_{t_a t_j} \psi_{t_j}^{j \rightarrow a} \prod_{j \in \partial a} \sum_{t_j} (1 - q_{t_a t_j}) \psi_{t_j}^{j \rightarrow a}.
\end{aligned} \tag{A2}$$

Since we have nonzero interactions between every pair of nodes, in Eq. A1 we have totally  $n(n-1) + 2mn$  messages. However, this gives an algorithm where even a single update takes  $O(n^2)$  time, making it suitable only for networks of up to a few thousand nodes. Happily, for large sparse networks, i.e., when  $n, m$  is large and  $p_{t_i t_j} = q_{t_i t_j} = O(1/n)$ , we can neglect terms of sub-leading order in the equations. In that case we can assume that  $i$  or  $a$  sends the same message to all its non-neighbors  $j$ , and treat these messages as an external fields, thus we only need to keep track of  $2M$  messages where  $M$  is the number of all edges (edges and hyperedges), and finally each update step takes on  $O(n)$  time.

Suppose that  $j \notin \partial i$ , we have :

$$\begin{aligned} \psi_{t_i}^{i \rightarrow j} &= \frac{\alpha_{t_i}}{Z^{i \rightarrow j}} \prod_{k \in \partial i} \sum_{t_k} p_{t_i t_k} \psi_{t_k}^{k \rightarrow i} \prod_{k \notin \partial i \setminus j} (1 - \sum_{t_k} p_{t_i t_k} \psi_{t_k}^{k \rightarrow i}) \\ &\cdot \prod_{a \in \partial i} \sum_{t_a} q_{t_i t_a} \psi_{t_a}^{a \rightarrow i} \prod_{a \notin \partial i} (1 - \sum_{t_a} q_{t_i t_a} \psi_{t_a}^{a \rightarrow i}) \\ &= \psi_{t_i}^i + O(1/n) \end{aligned} \quad (\text{A3})$$

Similarly,  $\psi_{t_a}^{a \rightarrow i} = \psi_{t_a}^a + O(1/m)$ , hence the messages on non-edges do not depend to leading order on the target node. For nodes with  $j \in \partial i$ , we have

$$\begin{aligned} \psi_{t_i}^{i \rightarrow j} &= \frac{\alpha_{t_i}}{Z^{i \rightarrow j}} \prod_{k \in \partial i \setminus j} \sum_{t_k} p_{t_i t_k} \psi_{t_k}^{k \rightarrow i} \prod_{k \notin \partial i} (1 - \sum_{t_k} p_{t_i t_k} \psi_{t_k}^{k \rightarrow i}) \\ &\cdot \prod_{a \in \partial i} \sum_{t_a} q_{t_i t_a} \psi_{t_a}^{a \rightarrow i} \prod_{a \notin \partial i} (1 - \sum_{t_a} q_{t_i t_a} \psi_{t_a}^{a \rightarrow i}) \\ &\simeq \alpha_{t_i} \frac{e^{-h_{t_i}}}{Z^{i \rightarrow j}} \prod_{k \in \partial i \setminus j} \sum_{t_k} p_{t_i t_k} \psi_{t_k}^{k \rightarrow i} \prod_{a \in \partial i} \sum_{t_a} q_{t_i t_a} \psi_{t_a}^{a \rightarrow i} \end{aligned} \quad (\text{A4})$$

where we have neglected terms that contribution  $O(1/n)$  and  $O(1/m)$  to  $\psi_{t_i}^{i \rightarrow j}$ , and defined an auxiliary external field

$$h_{t_i} = \sum_k \sum_{t_k} p_{t_i t_k} \psi_{t_k}^k + \sum_a \sum_{t_a} q_{t_i t_a} \psi_{t_a}^a \quad (\text{A5})$$

Applying the same approximation to the external fields acting on feature nodes, we can finally arrive at (4).

### Appendix B: deriving the detectability transition using noise perturbations

On graphs generated by the JSBM, the probability that a graph node has  $k_1$  neighboring graph nodes follows a Poisson distribution  $p_1(k_1)$  with average degree  $c_1$ . And the probability of having  $k_2$  features follows a Poisson distribution  $p_2(k_2)$  with average degree  $c_2$ . Similarly, the probability that a feature node has  $k_3$  neighboring nodes follows a Poisson distribution  $p_3(k_3)$  with average degree  $nc_2/m$ . Considering a branching process on a graph generated by the JSBM with infinite size, the

average branching ratio of the process is related to the excess degree which is defined using the average number of neighbors based on having a neighbor. The average excess degree is computed as

$$\tilde{c}_1 = \frac{\sum_{k_1} k_1(k_1-1)p_1(k_1)}{\sum_{k_1} k_1 p_1(k_1)} = c_1 \quad (\text{B1})$$

Similarly, the excess degree of feature nodes are

$$\tilde{c}_3 = \frac{\sum_{k_2} p_2(k_2)k_2(k_2-1)n/m}{\sum_{k_2} k_2 p_2(k_2)} = c_2 n/m = c_3. \quad (\text{B2})$$

and similarly,  $\tilde{c}_2 = c_2$ . Let us consider a noise propagation process in a tree as depicted in Fig. 2, with number of depth  $l \rightarrow \infty$ . In the tree, odd layers contain solely graph nodes, and even layers contain solely feature nodes (hyperedge, blue boxes) and edges (green boxes) which connect graph nodes in odd layers. Assume that on the leaves of the tree (nodes on the  $l$  layer) the paramagnetic fixed point is perturbed as

$$\psi_{t_{v_l}}^{v_l \rightarrow v_{l-1}} = \alpha_{t_{v_l}} + \delta_{t_{v_l}}^{v_l \rightarrow v_{l-1}}. \quad (\text{B3})$$

where  $v_l$  represent graph node on the  $l$  layer,  $t_{v_l}$  is label of  $v_l$ ,  $v_0$  corresponds to root node  $i$  in Fig. 2. Now let us investigate influence of perturbation of message on any leaf, to the message on the root of the tree. First choose one path only containing graph node s(i.e., nodes are not connected by feature nodes) for simplicity and latter generalize to paths containing feature nodes or hyperedges, we define Jacobian matrix  $\mathbf{T}^{i \rightarrow j}$  with respect to messages passing from a graph node  $i$  to another graph node  $j$  along an edge  $(ij)$ , and the Jacobian matrix  $\mathbf{T}^{a \rightarrow i}$  corresponding to message passing from a feature node  $a$  to a graph node  $i$ , together with the third matrix  $\mathbf{T}^{i \rightarrow a}$ . The elements of the Jacobian matrices are computed as

$$\begin{aligned} T_{t_i t_k}^{i \rightarrow j} &= \frac{\partial \psi_{t_j}^{j \rightarrow k}}{\partial \psi_{t_i}^{i \rightarrow j}} \Big|_{\alpha_{t_i}} = \alpha_{t_i} \left( \frac{np_{t_i t_k}}{c_1} - 1 \right), \\ T_{t_a t_i}^{a \rightarrow i} &= \frac{\partial \psi_{t_i}^{i \rightarrow j}}{\partial \psi_{t_a}^{a \rightarrow i}} \Big|_{\alpha_{t_a}, \beta_{t_i}} = \alpha_{t_i} \left( \frac{mq_{t_a t_i}}{c_2} - 1 \right), \\ T_{t_i t_a}^{i \rightarrow a} &= \frac{\partial \psi_{t_a}^{a \rightarrow j}}{\partial \psi_{t_i}^{i \rightarrow a}} \Big|_{\alpha_{t_i}, \beta_{t_a}} = \beta_{t_a} \left( \frac{mq_{t_i t_a}}{c_2} - 1 \right). \end{aligned} \quad (\text{B4})$$

these matrices represent propagation strength (4) between any two messages in the vicinity of the paramagnetic fixed point. we can see that all these matrices are independent on node indices, and only depend on what node type of the two nodes connected or propagated to. If the path only contains edges, i.e. without hyperedges, the perturbation  $\delta_{t_{v_0}}^{v_0 \rightarrow x}$  of the root node induced by the perturbation  $\delta_{t_{v_l}}^{v_l \rightarrow v_{l-1}}$  can be written as

$$\delta_{t_{v_0}}^{v_0 \rightarrow x} = \sum_{\{t_{v_d}: d=1, \dots, l\}} \prod_{d=0}^{l-1} T_{t_{v_d}, t_{v_{d+1}}}^{i \rightarrow j} \delta_{t_{v_l}}^{v_l \rightarrow v_{l-1}} \quad (\text{B5})$$

or in a vector form,  $\delta^{v_0 \rightarrow x} = (\mathbf{T}^{i \rightarrow j})^l \delta^{v_l \rightarrow v_{l-1}}$ . Now consider the path contains both edges and hyper edges: every step passing through a hyper edge,  $\mathbf{T}^{i \rightarrow a}$  and  $\mathbf{T}^{a \rightarrow i}$  transmits to  $\mathbf{T}^{i \rightarrow j}$ , therefore, the total weights acting on the path is

$$\delta^{v_0 \rightarrow x} = (\mathbf{T}^{i \rightarrow j})^s (\mathbf{T}^{i \rightarrow a} \mathbf{T}^{a \rightarrow i})^{(l-s)} \delta^{v_l \rightarrow v_{l-1}}$$

where  $s$  is the number of edge, and  $l - s$  is the number of hyperedge or graph node on this path.

At the limit  $l \rightarrow \infty$ ,  $(\mathbf{T}^{i \rightarrow j})^s (\mathbf{T}^{i \rightarrow a} \mathbf{T}^{a \rightarrow i})^{(l-s)}$  is dominated by product of the largest eigenvalues,  $\lambda_1$ ,  $\lambda_2$ , and  $\lambda_3$  of the three matrices, also notice that  $\lambda_2 = \lambda_3$ . So the above equation can be written as

$$\delta^{v_0 \rightarrow x} = (\lambda_1)^s (\lambda_2)^{2(l-s)} \delta^{v_l \rightarrow v_{l-1}}.$$

Now let us consider the collection of all perturbations on the root node  $v_0$  from all leaves. Obviously the mean is 0, and the variance on component  $t$  of the perturbation vector is computed as

$$\begin{aligned} & \langle (\delta_t^{v_0 \rightarrow x})^2 \rangle \\ &= \left\langle \left( \sum_{s=0}^l \sum_1^{\binom{l}{s}} (c_1)^s (c_2 c_3)^{l-s} \sum_{v_l=0} \lambda_1^s \lambda_2^{2(l-s)} \delta^{v_l \rightarrow v_{l-1}} \right)^2 \right\rangle \\ &= \sum_{s=0}^l \sum_1^{\binom{l}{s}} (c_1)^s (c_2 c_3)^{l-s} \sum_{v_l=0} \lambda_1^{2s} \lambda_2^{4(l-s)} \langle (\delta_t^{v_l \rightarrow v_{l-1}})^2 \rangle \\ &= \sum_{s=0}^l \binom{l}{s} (c_1 \lambda_1^2)^s (c_2 c_3 \lambda_2^4)^{l-s} \langle (\delta_t^{v_l \rightarrow v_{l-1}})^2 \rangle \\ &= (c_1 \lambda_1^2 + c_2 c_3 \lambda_2^4)^l \langle (\delta_t^{v_l \rightarrow v_{l-1}})^2 \rangle. \end{aligned} \quad (\text{B6})$$

Here, we have made use the property that all perturbations on different leaves are independent. Obviously, the paramagnetic fixed point is locally unstable under random perturbation when  $(c_1 \lambda_1^2 + c_2 c_3 \lambda_2^4)^l > 1$ , so the phase transition of detectability locates at

$$c_1 \lambda_1^2 + c_2 c_3 \lambda_2^4 = 1. \quad (\text{B7})$$

### Appendix C: Conventional graph convolution networks and the spectral localization problem of the linear convolution kernels in large sparse networks

Convolution networks [37] have been proved to be the most successful model for image classifications [38] and many other machine learning problems [2]. The success of CNN is credited to the convolution which is a linear operator defined on grid-like structures. Recently, significant amount of attention has been paid on generalizing convolution operations to graphs, which does not have any grid structure.

In [39], authors propose to define convolution layer on graphs operating on spectrum of the graph Laplacian using its eigenvectors:

$$\mathbf{X}_{l+1} = \sigma(\Lambda \star \mathbf{X}_l) = \sigma(\mathbf{V} \Lambda \mathbf{V}^T \mathbf{X}_l), \quad (\text{C1})$$

where  $\mathbf{X}_l$  is activation in the  $l^{\text{th}}$  layer,  $\mathbf{V}$  is the matrix of eigenvectors of graph Laplacian  $\mathbf{L} = \mathbf{I} - \mathbf{D}^{-\frac{1}{2}} \mathbf{A} \mathbf{D}^{-\frac{1}{2}}$  ( $n$  is the number of nodes and  $\mathbf{D}$  is the diagonal matrix containing degrees), and  $\sigma(\cdot)$  is an element-wise non-linear activation function, and  $\Lambda$  is a diagonal matrix representing a kernel in the frequency (graph Fourier) domain. Usually  $\Lambda$  contains only several non-zero elements, working as cut-off to the frequency in the Fourier domain, because it is believed that only few eigenvectors of graph Laplacian are enough for describing smooth structures of the graph. It is also in consideration of the computational efficiency as computing leading eigenvectors.

Even though, computing a few eigenvectors of the Laplacian of large graphs could be quite heavy. In [40], authors proposed to parametrize the kernel in the frequency domain by truncated expansion using Chebyshev polynomials up to  $K$ -th order:

$$\mathbf{X}_{l+1} = \sigma(\Lambda \star \mathbf{X}_l) \approx \sigma \left[ \sum_{k=0}^K c_k T_k \left( \frac{2}{\lambda_{\max}} \mathbf{L} - \mathbf{I} \right) \mathbf{X}_l \right], \quad (\text{C2})$$

where  $c_k$  denotes coefficients,  $T_K(x) = 2xT_{K-1}(x) - T_{K-2}(x)$  are recursively defined Chebyshev polynomials, and  $\lambda_{\max}$  is the largest eigenvalue. [1] limited the convolution operation to  $K = 1$ , and approximate  $\lambda_{\max} = 2$ , then obtain

$$\mathbf{X}_{l+1} = \sigma(\Lambda \star \mathbf{X}_l) \approx \theta_1 X - \theta_2 D^{-\frac{1}{2}} \mathbf{A} D^{-\frac{1}{2}},$$

with two free parameters  $\theta_1$  and  $\theta_2$ . Further, [1] restricted two parameters by specifying  $\theta = \theta_1 = \theta_2$ , and introduced a normalization trick

$$\mathbf{I} + \mathbf{D}^{-\frac{1}{2}} \mathbf{A} \mathbf{D}^{-\frac{1}{2}} \rightarrow \widehat{\mathbf{D}}^{-\frac{1}{2}} \widehat{\mathbf{A}} \widehat{\mathbf{D}}^{-\frac{1}{2}},$$

where  $\widehat{\mathbf{A}} = \mathbf{A} + \mathbf{I}$ , and  $\widehat{D}_i = 1 + \sum_j A_{ij}$ . Finally by generalizing to node feature of  $\kappa$  components, that is, to  $\kappa$  channel signal  $\mathbf{X} \in \mathbb{R}^{n \times \kappa}$ , one arrives at GCN[1] with forward model taking the form of

$$\mathbf{X}_{l+1} = \sigma(\widetilde{\mathbf{A}} \mathbf{X}_l \mathbf{W}), \quad (\text{C3})$$

where  $\sigma(\cdot)$  is an activation function such as ReLU,  $\mathbf{X}_{l+1} \in \mathbb{R}^{n \times \kappa_l}$  is the network state at layer  $l$ ,  $n$  denotes number of nodes in the graph,  $\kappa_l$  is the dimension of state at layer  $l$ . The matrix  $\mathbf{W} \in \mathbb{R}^{\kappa_{l+1} \times \kappa_l}$  is the trainable weight matrix at  $l$ -th layer, and propagator  $\widetilde{\mathbf{A}}$  (18) is responsible for convolving the neighborhood of a node, and should be shared over the whole network.

It has been shown in [1] that GCN significantly outperforms related methods. These include manifold regularization (ManiReg) [41], Semi-supervised embedding (SemiEmb) [42], Label Propagation (LP) [43], skip-gram

based graph embedding (DeepWalk) [44], iterative classification algorithm in conjunction with two classifiers taking care of both local node features and aggregations [45], and recently proposed Planetoid [42].

In the GCN and many further developments in recent years, almost all of them can be understood as an effective object representation started from original feature vector then projected by finite power times of the linear convolution kernel. So we recognize that the main principle of the graph convolutions kernels is inspired by spectral properties of linear operators such as Laplacians, normalized Laplacians [1, 31], random walk matrix [3] etc. The assumptions behind is that eigenvectors of the the graph convolution kernel contains information about global group label, and can be revealed during forward propagation in GCNs.

However it is known that this assumption does not hold in large sparse networks because eigenvectors of conventional linear operators such as graph Laplacians have localization problem, due to fluctuation of degrees or local structures of the graph [26, 32]. Even on random graphs where the Poisson degree distribution is rather concentrated, the localization problem is still significant on large graphs. For the adjacency matrix, it is well known that the largest eigenvalues is bounded below by squared root of the maximum degree (which grows as  $\frac{\log(n)}{\log \log(n)}$ ), and diverges on large graphs when number of nodes  $n \rightarrow \infty$ . The corresponding eigenvectors only report information of largest degrees. For normalized matrices such as normalized Laplacian, there are many eigenvalues that are very close to 0, with corresponding eigenvectors reporting information about local dangling sub-graphs rather than global structures related to group labels. We refer to [26, 32] for detailed analysis of spectrum localizations of graph Laplacians, and for comparisons between spectral algorithms using different operators in large sparse graphs. Unfortunately real-world networks are usually sparse, as we can see from Table I that (although they are not large enough) the citation networks we used for experiments are all have average degree around 4, which is quite low.

In large synthetic networks the sparsity issue for conventional GCNs is revealed more clearly. In Fig. 6 we carried out extensive experiments to verify our analysis.

#### Appendix D: Belief Propagation Graph Convolution Network(BPGCN)

On a graph with  $n$  graph nodes,  $m$  features nodes,  $nc_1$  edges and  $nc_2$  hyper edges, i.e. average degree of the graph nodes in the uni-partite is  $c_1$  and average degree of graph nodes in the bi-partite graph is  $c_2$ . We define matrices storing cavity messages  $\Psi_l^{i \rightarrow j} \in \mathbb{R}^{nc_1 \times \kappa}$ ,  $\Psi_l^{i \rightarrow a} \in \mathbb{R}^{nc_2 \times \kappa}$  and  $\Psi_l^{a \rightarrow i} \in \mathbb{R}^{nc_2 \times \kappa}$ , and marginal matrix  $\Psi_l^i \in \mathbb{R}^{n \times \kappa}$  and  $\Psi_l^a \in \mathbb{R}^{m \times \kappa}$ , where the subscript  $l$  represent the cavity messages after  $l$ - step iteration of belief propagation equations (4), the belief propagation

can be written in the form of matrix multiplications:

$$\begin{aligned} \Psi_{l+1}^a &= \text{Softmax} \left[ \mathbf{E} \log(\Psi_l^{i \rightarrow a} \mathbf{P}) \right] \\ \Psi_{l+1}^i &= \text{Softmax} \left[ \mathbf{H} \log(\Psi_l^{a \rightarrow i} \mathbf{Q}) + \mathbf{C} \log(\Psi_l^{i \rightarrow j} \mathbf{P}) \right] \\ \Psi_{l+1}^{i \rightarrow j} &= \text{Softmax} \left[ \mathbf{N} \log(\Psi_l^{a \rightarrow i} \mathbf{Q}) + \mathbf{B} \log(\Psi_l^{i \rightarrow j} \mathbf{P}) \right] \\ \Psi_{l+1}^{i \rightarrow a} &= \text{Softmax} \left[ \mathbf{M} \log(\Psi_l^{i \rightarrow j} \mathbf{P}) + \mathbf{R} \log(\Psi_l^{a \rightarrow i} \mathbf{Q}) \right] \\ \Psi_{l+1}^{a \rightarrow i} &= \text{Softmax} \left[ \mathbf{D} \log(\Psi_l^{i \rightarrow a} \mathbf{Q}) \right] \end{aligned} \quad (\text{D1})$$

where  $\mathbf{P}$ ,  $\mathbf{Q}$  are affinity matrices of size  $\kappa \times \kappa$ . Matrices  $\mathbf{E}$ ,  $\mathbf{H}$ ,  $\mathbf{C}$ ,  $\mathbf{N}$ ,  $\mathbf{B}$ ,  $\mathbf{M}$ ,  $\mathbf{R}$  and  $\mathbf{D}$  stand for the nonbacktracking matrix [26], which are defined as follows.

$$\begin{aligned} \mathbf{E}_{a,i \rightarrow b} &= \delta_{ab} \in \{0, 1\}^{m \times nc_2} \\ \mathbf{H}_{i,a \rightarrow j} &= \delta_{ij} \in \{0, 1\}^{n \times nc_2} \\ \mathbf{C}_{i,k \rightarrow l} &= \delta_{il} \in \{0, 1\}^{n \times nc_1} \\ \mathbf{N}_{i \rightarrow j, a \rightarrow l} &= \delta_{il}(1 - \delta_{aj}) \in \{0, 1\}^{nc_1 \times nc_2} \\ \mathbf{B}_{i \rightarrow j, k \rightarrow l} &= \delta_{il}(1 - \delta_{kj}) \in \{0, 1\}^{nc_1 \times nc_1} \\ \mathbf{M}_{i \rightarrow a, j \rightarrow l} &= \delta_{il}(1 - \delta_{aj}) \in \{0, 1\}^{nc_2 \times nc_1} \\ \mathbf{R}_{i \rightarrow a, b \rightarrow l} &= \delta_{il}(1 - \delta_{ab}) \in \{0, 1\}^{nc_2 \times nc_2} \\ \mathbf{D}_{a \rightarrow i, j \rightarrow b} &= \delta_{ab}(1 - \delta_{ij}) \in \{0, 1\}^{nc_2 \times nc_2}. \end{aligned} \quad (\text{D2})$$

Therefore the matrix multiplication form of parallelly updated belief propagation can be seen as a forward model of a neural network. We expand above equation and truncat eafter  $L$  steps of iterations, we then call the obtained algorithm BPGCN with  $L$  layers. The states of the last layer is extracted out as output of the BPGCN for computing the cross entropy loss on training labels (16). The matrix  $\mathbf{Q}$  and  $\mathbf{P}$  are trainable parameters of the BPGCN and are updated using back propagation algorithm. We set input of our neural network using probability-normalized random initial cavity and marginals. In order to accelerate the training process of the BPGCN, we use an adjustable external field strength  $\gamma$  as hyper parameters. For example, suppose node  $i$  is in the training set, i.e. we have label  $t_i$  for node  $i$ , a term  $\gamma \log(0.1, 0.1, 0.9, \dots, 1)$  is added to (D1) inside the Softmax function. When  $\gamma$  approaches infinity, node  $i$  is pinned to label  $t_i$  [12], and is used as an hyper parameters adjusted using the validation set. For nodes in the training set, the cavity probabilities and marginals are initialized as  $(0, 1, \dots, 0)$ . So totally the parameters of BPGCN are  $\mathbf{P}$  and  $\mathbf{Q}$ , the hyper parameters are  $\epsilon_1$ ,  $\epsilon_2$ , and  $\gamma$ . The hyper parameters we used during the numerical experiments we have carried out on real-world datasets (in producing Tag. I are listed as follows: For CITESEER and CORA, we set neural network layers  $L = 5$  and external strength  $\gamma = 2.0$ ; on CORA we set  $\epsilon_1 = 0.1$ ,  $\epsilon_2 = 0.6$ ; on CITESEER we set  $\epsilon_1 = 0.1$ ,  $\epsilon_2 = 0.5$ . For PUBMED, we set  $L = 2$  layers, external strength  $\gamma = 1.5$ ,  $\epsilon_1 = 0.3$ , and  $\epsilon_2 = 0.8$ . For KARATE CLUB network and POLITICAL BLOGS network, we both set neural network layers  $L = 5$ , external strength  $\gamma = 0.5$ , and  $\epsilon_1 = 0.1$ .

### Appendix E: more comparisons on synthetic networks

In this section, we carry out extensive numerical experiments on synthetic networks generated by the JSBM with various continuously tuned parameters. The overlap of BP, BPGCN, GCN, APPNP, GAT and SGCN are compared against each other in Fig.6. In the top row, the average degree of the uni-partite graph is fixed to  $c_1 = 4, 6$ , and 10 from left to right. We can see that due to spectrum localizations of graph Laplacians as we have argued, when  $c_1$  is fixed to 4, GCN, APPNP, GAT, and SGCN work much worse than BPGCN, even when  $c_2$  is really large. We also see that when  $c_1$  is large, most of the graph convolution networks work well even at a very low  $c_2$  regime. In the second row of Fig.6, the average degree of the bipartite graph  $c_2$  is fixed and  $c_1$  varies. The figure shows that performance of GCNs approaches BPGCN, when  $c_1$  gradually increases.

In the third row of the figure,  $c_1, c_2$  and  $\epsilon_1$  are fixed and  $\epsilon_2$  varies. In the left panel,  $c_1 = c_2 = 4, \epsilon_1 = 0.1$ . The graphs are in the sparse regime so conventional GCNs do not work well because of the sparsity. In the middle panel,  $c_1 = c_2 = 10, \epsilon_1 = 0.4$ , so the graphs are not sparse, but the edges contains relatively low information about the labels. The results show that SGCN has trouble in this regime even when  $\epsilon_2$  is really small. In the right panel  $c_1 = c_2 = 10$ , and  $\epsilon_1 = 0.1$ , so the graphs are not in the sparse regime, and edges contain enough information about labels. We see that all GCNs except the APPNP performs reasonably well, but the APPNP has trouble with lower  $\epsilon_2$ , may be because an non-optimal  $\omega$  parameter was learned.

In the last row of the figure,  $c_1, c_2$ , and  $\epsilon_2$  are fixed, and the inverse signal-to-noise ratio  $\epsilon_1$  (on the uni-partite part) varies. In the left panel,  $c_1 = c_2 = 4, \epsilon_2 = 0.1$ , we see that BPGCN starts to have a large variance, but the overlap is on average much higher than other GCNs, due to the sparsity of the graphs. In the middle panel,  $c_1 = c_2 = 10, \epsilon_2 = 0.4$ , meaning that the hyper edges in the bipartite graph contain little information of the labeling, and main information come from the unipartite graph which is not sparse. In this case we see that the conventional GCNs works comprative to BP and BPGCN, because there is no sparsity issue. On the right panel,  $c_1 = c_2 = 10$ , and  $\epsilon_2 = 0.1$  which means that there is no sparsity issue for conventional GCNs, and the bipartite graph contains enough information about the ground-true labels. However the result is quite surprising, as when BP and BPGCN gives almost 100% accuracy in the full range of  $\epsilon_1$ , the conventional GCNs do not, gives very low accuracy with  $\epsilon_1$  is larger than 0.5. This phenomenon means when the edges of the graph are quite noisy, information from the features are not

extracted very well by the conventional GCNs.

To understand the reason, in Fig. 5 we plot training process of the GCN, MLP and BPGCN on a graph generated with  $c_1 = c_2 = 10, \epsilon_1 = 1, \epsilon_2 = 0.1$ . In this case  $\epsilon_1 = 1$

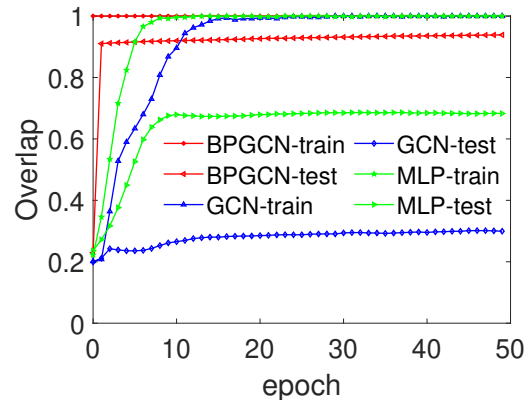


FIG. 5. Train and test overlap (Eq. (14)) as a function of epoch on a synthetic graph generated by the JSBM with  $n = m = 10000, c_1 = c_2 = 10, \epsilon_1 = 1$ , and  $\epsilon_2 = 0.1$ .

means that the uni-partite part of the graph is a pure random graph, with edges containing no information of the label. while  $\epsilon_2 = 0.1$  is quite high, itself contains ad-equit informatino about ground-true labels. The Fig. 5 shows that the BPGCN gives very high accuracy on the training set and test set even at beginning, because the  $\epsilon_2$  is so small that the initial condition for the BPGCN is already good. At begining of the training, the Multi-layer perceptron results (MLP) gives low training accuracy as well as low test accuracy. But after several steps of training, the training accuracy of the MLP goes to 1, and it generalizes very well to the test set on which the accuracy gradually increases to about 0.6. However this generalization does not happen on the GCN, as we can see that although GCN fits very well the training set, the test overlap is only slightly above 0.2, the results of random guess. Obviously, GCN overfit to train datasets. The reason for the overfitting is that the GCN always assumes that edges contain information of the labelings, even when the graph is a random graph.

Another information we can extract directly from the formula of the APPNP (20) is that, since APPNP uses ratios  $\omega$  and  $1 - \omega$  to weight contributions of edges and feature, the best results given by APPNP on the graphs where edges contain no information, and features contain all the information, is to the multi-layer perceptron. Indeed we have tested that with  $\epsilon_1 = 1, \epsilon_2 = 0.1, c_1 = c_2 = 10$ , the APPNP achieves overlap about 0.6 while MLP achieves 0.66.

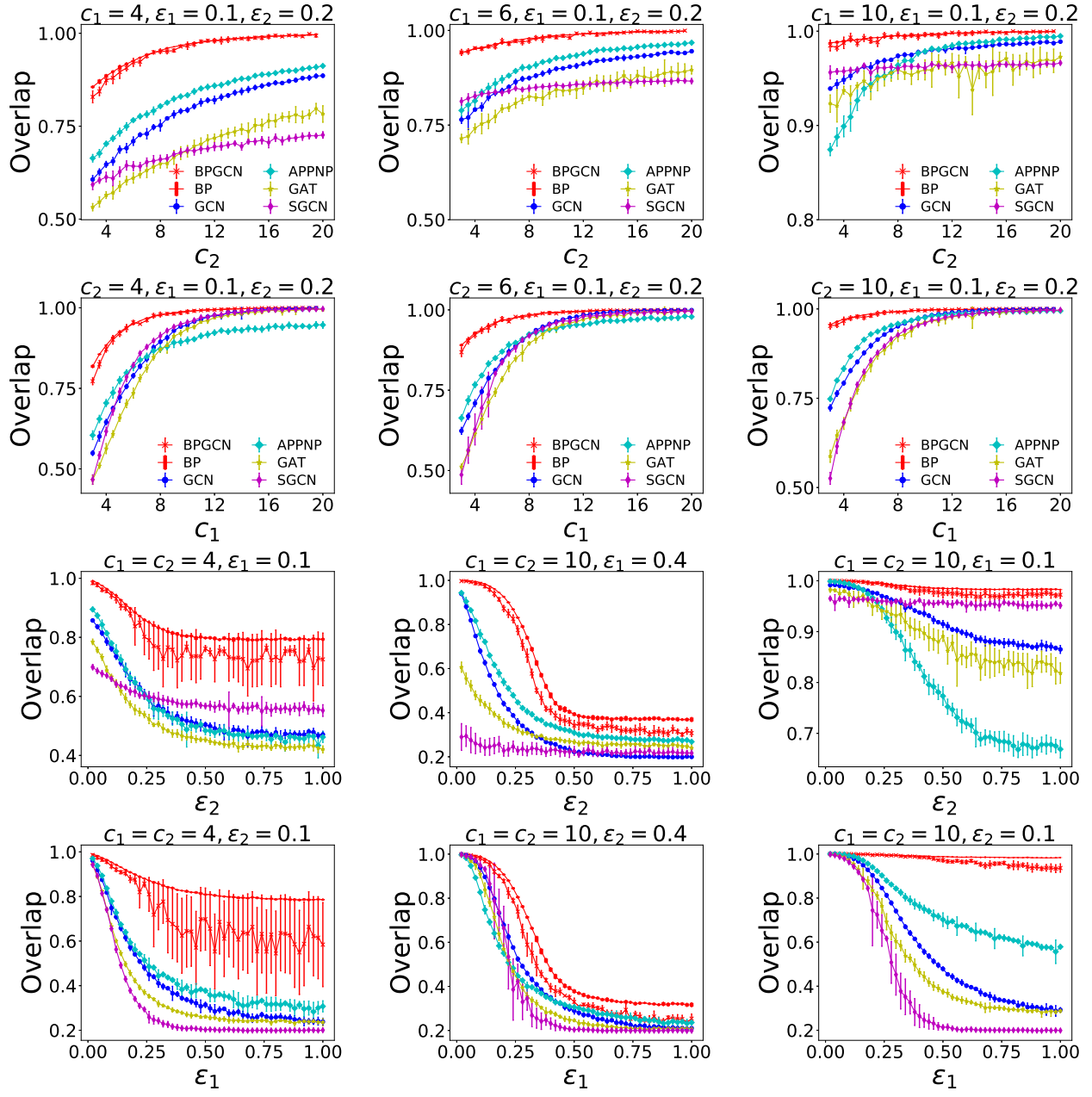


FIG. 6. Overlap (Eq. (14)) obtained by BP and various GCNs on synthetic networks generated by the JSBM with various of parameters. All networks are generated with  $n = m = 10000$ , and group numbers  $\kappa = 5$ , ratio of training labels  $\rho = 0.05$ . Each data point is averaged over 10 random instances. The parameters of graphs are printed on the title of each panel.